Geophysical Research Letters

RESEARCH LETTER
10.1029/2023GL103843

On the Particle Motion in Paleo-Magnetosphere During the Geomagnetic Polarity Reversal

Fan Gong[1,2], Yiqun Yu[1,2], Kun Bai[1,2], Jinbin Cao[1,2], and Yong Wei[3]

[1]School of Space and Environment, Beihang University, Beijing, China, [2]Key Laboratory of Space Environment Monitoring and Information Processing, Ministry of Industry and Information Technology, Beijing, China, [3]Institute of Geology and Geophysics, Chinese Academy of Sciences, Beijing, China

Key Points:

- We simulated charged particles' trajectories in the magnetosphere during the Matuyama-Brunhes reversal
- Particles cannot be "trapped" in an irregular magnetosphere
- The irregular geomagnetic field results in global particle precipitation

Supporting Information:

Supporting Information may be found in the online version of this article.

Correspondence to:

Y. Yu and J. Cao,
yiqunyu17@gmail.com;
jbcao@buaa.edu.cn

Citation:

Gong, F., Yu, Y., Bai, K., Cao, J., & Wei, Y. (2023). On the particle motion in paleo-magnetosphere during the geomagnetic polarity reversal. *Geophysical Research Letters*, *50*, e2023GL103843. https://doi.org/10.1029/2023GL103843

Received 24 MAR 2023
Accepted 3 JUN 2023

Author Contributions:

Data curation: Fan Gong
Formal analysis: Fan Gong
Investigation: Fan Gong, Yiqun Yu, Jinbin Cao, Yong Wei
Methodology: Fan Gong, Yiqun Yu, Kun Bai
Software: Yiqun Yu, Kun Bai
Visualization: Fan Gong
Writing – original draft: Fan Gong
Writing – review & editing: Yiqun Yu, Jinbin Cao

Abstract During the Earth's magnetic reversal, the dipole component of the magnetic field weakens, and the non-dipole component becomes dominant, resulting in a far more complex magnetospheric topology than that of a dipole. In this study, we used a particle tracing technique to investigate the motion of ions within an irregular magnetosphere during the Matuyama-Brunhes magnetic polarity reversal. Compared to the scenario in which the geomagnetic field is dominated by a dipole component, earthward-moving particles can be hardly "trapped" in the inner magnetosphere when the geomagnetic field experiences the polarity reversal, and particles can directly precipitate into the Earth's atmosphere on a global scale. It suggests that under an irregular magnetospheric configuration, the traditional trapped region of particles (e.g., radiation belt or ring current) no longer exists.

Plain Language Summary During the Earth's paleomagnetic reversal, the strength of the Earth's magnetic field was approximately 10% of its current value, accompanied by a weakening of the dipole component and an enhancement of the non-dipole component. Under the superposition of this non-axisymmetric multipole magnetic field, the magnetospheric structures may undergo significant changes. How charged particles travel in such an irregular magnetosphere and how different their trajectories are compared to the well-known textbook scenario are still unknown. In this study, by utilizing global MHD simulations and test-particle tracing techniques, we trace the charged particle's trajectory within the magnetosphere during the Matuyama-Brunhes magnetic polarity reversal. We found that under an irregular magnetosphere in the middle stage of the geomagnetic reversal, particles in the inner magnetosphere cannot be constantly trapped around the Earth. The traditional trapped region (e.g., radiation belt or ring current) no longer exists. Particles moving Earthward do not gain the same acceleration effect as those under the present-day magnetic field topology, resulting in a globally distributed pattern of particle precipitation. These differences can affect the global energy deposition and particle distribution in near-Earth space.

1. Introduction

The Earth's intrinsic magnetic field is generated in the outer core and extends several Earth radii into space. The magnetosphere is formed after the geomagnetic field interacts with the solar wind, protecting the Earth from the Sun and high-energy particles from the cosmos (Glassmeier & Vogt, 2010; Jackson & Finlay, 2007; Korte & Mandea, 2019). The current geomagnetic field can be approximated by a dipole centered at the Earth's core with an axis inclined by about 11° to the rotational axis. This dipole contributes approximately 80% of the surface magnetic field, with the remaining 20% being non-dipolar (Merrill et al., 1997). Consequently, charged particles can repetitively bounce and drift around the Earth, leading to trapped populations in the inner magnetosphere. For example, Van Allen radiation belts in the current magnetosphere are filled with high-energy charged particles (Hudson et al., 2008). The trapped energetic particles can also form ring current around the Earth, which distorts the background magnetic field and changes the plasma motion.

The Earth's magnetic field is not static but rather constantly changing. Polarity reversals and shifts of the geomagnetic field have occurred many times in geological history (Cande & Kent, 1995; Laj & Channell, 2015; Lowrie & Kent, 2004; Singer, 2014). Over the years, there has been a significant improvement in understanding geomagnetic reversals through paleomagnetic studies and simulations of the Earth's dynamo (Jacobs, 2005; Valet & Fournier, 2016; Valet et al., 2012). During the geomagnetic polarity transition, the intensity of the geomagnetic field significantly decreases and is no longer dominated by a dipole (Amit et al., 2010; Channell et al., 2009;

Singer et al., 2005; Valet et al., 2005, 2012). Non-dipolar contributions, such as quadrupolar and octupolar components, strongly influence the topology of the magnetosphere (Korte et al., 2019; Leonhardt & Fabian, 2007; Singer et al., 2019) and hence the motion of charged particles. Stadelmann et al. (2010) tracked particles from outside the magnetosphere inward and examined the particle precipitation regions under quadrupole fields and dipole-quadrupole superpositions. Some other studies investigated the cut-off region of cosmic rays in more complex geomagnetic fields (Gao et al., 2022; Shea & Smart, 2004; Smart & Shea, 2009), but the detailed trajectories of the cosmic rays within the magnetosphere were not shown. Gong et al. (2022) performed global MHD simulations to study the solar wind-magnetosphere interactions during the Matuyama-Brunhes (M-B) magnetic polarity reversal. They found that the magnetospheric configuration in the middle stage of the polarity reversal is quite irregular, neither like purely quadrupolar nor octupolar structure. Their study showed that even under quiet solar wind conditions, the solar wind energy power transfer efficiency during the M-B reversal is higher than that during the post-reversal time. This indicates that the magnetosphere shielding effect is weakened during the M-B reversal, suggesting that the near-Earth space environment at that time would be greatly affected. Would ring currents, radiation belts, and other structures still exist? How charged particles travel in such an irregular magnetosphere and how different their trajectories are compared to the well-known "bounce-drift" trapping scenario are still unknown.

In this study, we utilize a test-particle tracing technique to investigate the motion of charged particles under different magnetospheric configurations during the M-B geomagnetic polarity reversal. We compare two cases, one with the Earth's magnetic field dominated by a dipole field and the other one with dominant multipole fields. Our results indicate that compared to the dipolar case, the traditional trapped region of particles, such as radiation belt or ring current, no longer exists under the irregular magnetosphere in the middle stage of the geomagnetic reversal. Particles moving toward the Earth either directly precipitate or return to the tail along magnetic field lines when approaching the Earth. Precipitation regions change from the traditional auroral zone to the entire Earth surface implying a significant impact on the Earth's upper atmosphere during this period. In addition, this work may also shed lights on the study of other planets with non-dipole intrinsic magnetic fields, such as Mars.

2. Methodology

To investigate the trajectories of charged particles within the magnetosphere, we use the Space Weather Modeling Framework (SWMF) (Tóth et al., 2005, 2012) to simulate the solar wind-magnetosphere interactions and obtain the corresponding magnetospheric configuration for the particle tracing. The SWMF integrates a global MHD model Block-Adaptive Tree Solar-wind Roe Upwind Scheme (BATS-R-US) (Powell et al., 1999) and an ionospheric potential solver (A. Ridley et al., 2004). It is suitable for solving the geospace circulation dynamics and has been extensively validated (e.g., Yu & Ridley, 2008; Yu et al., 2010, 2015; Welling & Ridley, 2010; A. J. Ridley et al., 2016, and others). The BATS-R-US model is implemented with an intrinsic geomagnetic field, which is characterized by a data-reconstructed model "IMMAB4" (Leonhardt & Fabian, 2007) and is used to determine the geomagnetic field at any epoch from 795 thousand years ago (ka) to 764 ka, covering the entire M-B reversal period. We choose two epochs for this study: one after the reversal (765 ka) and one during the reversal (774.5 ka), to obtain a dipolar configuration and an irregular configuration, respectively. The BATSR-U-S model is driven by constant solar wind conditions as follows: $V_{xsw} = 400$ km/s, $N_{sw} = 5$ cm^{-3}, $T = 10^5 K$, and the interplanetary magnetic field (IMF) $B_z = -10$ nT, while $V_{ysw} = V_{zsw} = 0$ km/s, and IMF B_x = IMF $B_y = 0$ nT. Simulations are run for 100,000 steps to reach a steady state of the magnetosphere. Details of the model set can be found in our previous study (Gong et al., 2022).

The test particle tracing technique allows for the calculation of the trajectory of charged particles in a global electromagnetic field environment. It is widely acknowledged that numerical methods for solving the motion of charged particles typically involve the solution of the Newton-Lorentz equations and the averaging of the particle gyroperiod under the guiding-center approximation, in which the first adiabatic invariant is conserved (Brizard & Chan, 1999; Cary & Brizard, 2009). Since Lorentz motion has a time scale of the electron gyroperiod, which is several orders of magnitude smaller than the bounce or drift periods of guiding center trajectories, the computation of the latter is much more efficient. However, the guiding-center approximation requires that the particle gyroperiod is much smaller than the time scale of the evolution of the electric and magnetic fields, and the gyroradius is much smaller than the characteristic gradient length scale of the fields. This requirement is sometimes not satisfied. Therefore, in this study, we introduce a parameter χ to determine the effectiveness of the guiding center approximation (Kress et al., 2007).

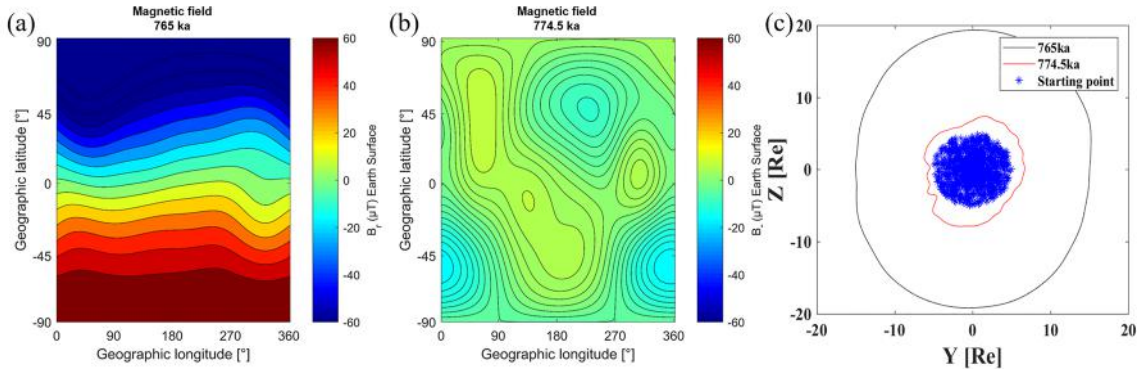

Figure 1. Panels (a) and (b) show the geographical maps of the Br component of the geomagnetic field at the Earth's surface during the post-reversal (765 ka) and the middle stage (774.5ka) of the M-B reversal respectively, adopted from Gong et al. (2022). Panel (c) shows the two magnetopause locations in the YZ plane at $X_{GSM} = -10$ Re at 765 ka (blue curve) and 774.5 ka (red curve), respectively. The asterisks represent charged particles initially released in the simulation for tracing within a $r = 5$ Re zone at $X_{GSM} = -10$ Re in the YZ plane.

$$\chi = \rho_{gyro} \frac{|\nabla B|}{B} \tag{1}$$

where ρ_{gyro} is the particle's gyroradius, B is the magnetic field strength, and $|\nabla B|$ is the norm of the ∇B tensor. In the code, particles are switched to Lorentz mode when $\chi \geq 0.5$. Details of the test-particle tracing technique can be found in Supporting Information S1.

Figures 1a and 1b, adopted from Gong et al. (2022), shows the intrinsic magnetic field component (B_r) in geographic coordinates for the two chosen epochs. After the M-B reversal at 765 ka, the geomagnetic field is more or less in a dipolar configuration. However, during the reversal time at 774.5 ka, the geomagnetic field shows multiple poles and is quite complex in its geographical distribution. The cross-section areas of the magnetopause shown in Figure 1c are greatly different. The magnetopause size in the middle stage of the reversal at 774.5 ka (indicated by the red line) is much smaller than that in the post-reversal time at 765 ka, represented by the blue line. The initial positions of ions, denoted as blue asterisks, are randomly distributed in the nightside YZ plane with a radius of 5 Re centered on the X axis at $X_{GSM} = -10$ Re. The ions constitute a Kappa distribution (with $\kappa = 5.6$) between 0.01 and 100 keV (Kirpichev et al., 2021, following their Figure S1) with random pitch angles between 0° and 180°. A total of 21,600 particles are released and traced. The simulations are run for 20 min or stop tracing the particle when it leaves the simulation domain ($X_{GSM} \in [-15, 15]$, $Y_{GSM} \in [-15, 15]$, $Z_{GSM} \in [-15, 15]$ or precipitates into the upper atmosphere).

3. Result

Figure 2a displays the trajectories of selected particles within the magnetosphere at 765 ka. At this epoch, ions entering the inner magnetosphere mainly exhibit westward drift motion, tending to form a drift shell (enclosed by the blue lines), which also signifies the existence of the radiation belt and ring current structure in the magnetosphere. It is also noted that a small portion of ions eventually precipitate into the Earth's atmosphere during the drift process (indicated by red lines).

We focus on the motion of charged particles that are able to enter the inner magnetosphere after passing through the boundary at $r = 6$ RE. According to their trajectories, these charged particles are categorized into two groups: "trapped" in the inner magnetosphere or "precipitated" into the Earth's atmosphere. The first group involves particles that traverse the boundary at $r = 6$ Re and are confined within the region between the Earth's atmosphere and the boundary, without precipitating into the Earth's atmosphere within the simulation time interval. We consider this type of particle to be "trapped" in the inner magnetosphere (group-1, Figure 2b). The second group encompasses particles that pass through the boundary and ultimately reach a height of 800 km above the Earth's surface within the simulation time. We consider these particles to be "precipitated" particles as they eventually precipitate into the Earth's atmosphere (group-2, Figure 2c).

Owing to the recovery of the dipole component after the M-B reversal, the magnetic field morphology at 765 ka is dipolar near the Earth, as shown in Figure 2d. Since the Earth's magnetic field is nearly north-south

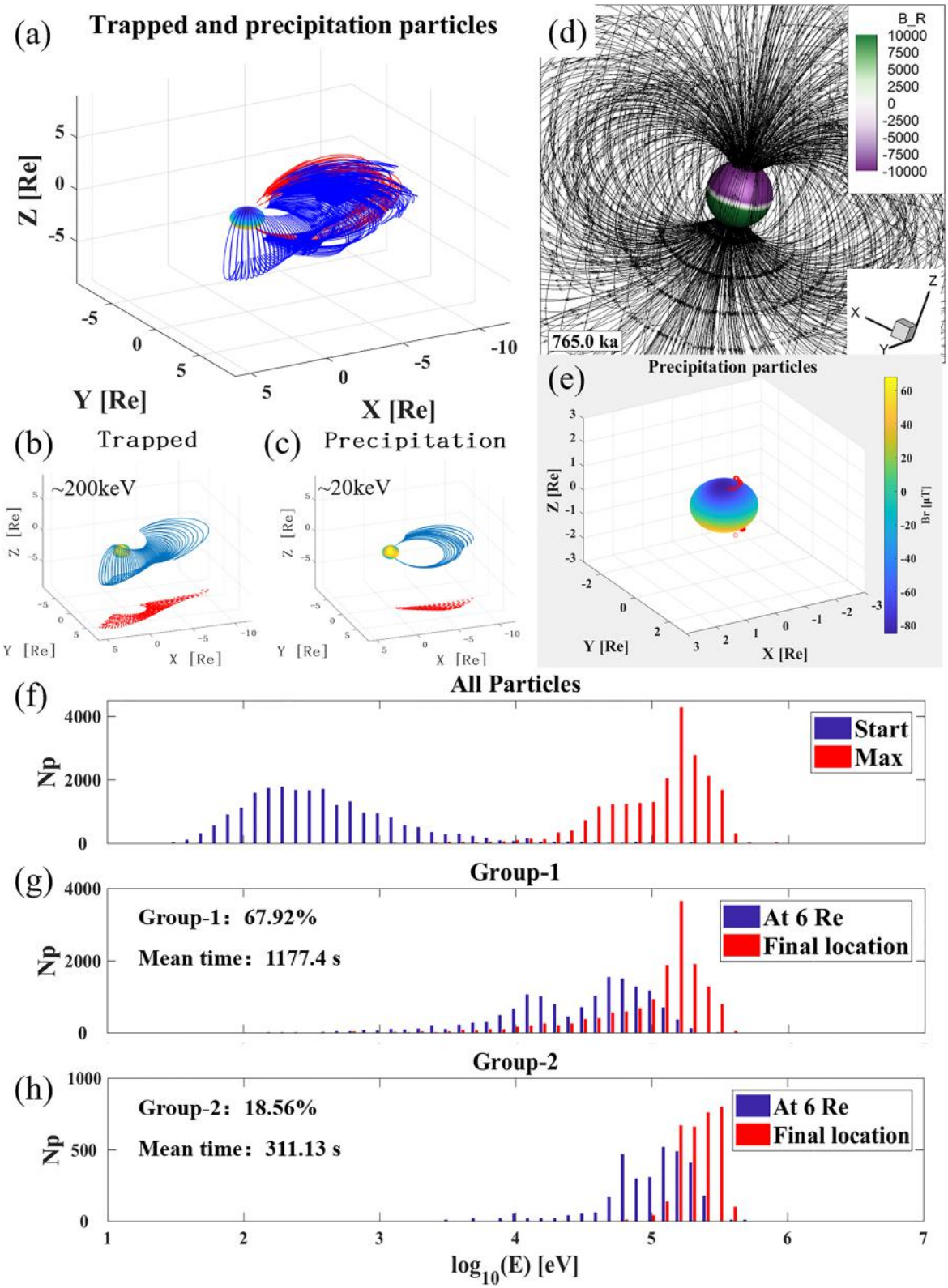

Figure 2.

axis-symmetric, the polar cap is formed at each pole after interacting with the southward IMF. Therefore, particles primarily precipitate in the high-latitude polar cap region, forming an auroral oval (as shown in Figure 2e by red circles).

Figure 2f presents the energy distribution of all particles at their initial locations, shown by the blue histogram. It follows our designated kappa distribution with characteristic energy at 100 eV, a typical temperature of the magnetotail plasma. As particles travel toward the Earth, particles gain energy. Their maximum energies during the motion are distributed in the red histogram, exhibiting clearly a bulk shift toward the high-energy tail. The maximum energy of these particles exceeds 100 keV. Figure 2g shows the energy distribution of "trapped" particles at $r = 6$ Re boundary (blue histogram) and at their final locations within the $r = 6$ Re sphere (red histogram). Their final location are recorded at the end of the simulation. These particles account for 67.92% of the total test particles, and the energy distribution at 6 Re significantly differs from that at initial locations, being much higher. This suggests that particles are accelerated while moving Earthward from the magnetotail. Electric drift (due to a large convection electric field on the nightside) may play a major role in the Earthward motion of particles as the Earth's magnetosphere is in a Dungey cycle mode under southward IMF conditions. Therefore, particles moving Earthward through the magnetic pileup region which is located downstream of the magnetic reconnection are accelerated. After entering the inner magnetosphere, these trapped particles exhibit drift motion around the Earth for 1,177.4 s, nearly occupying the entire simulation period, meaning that they spend most of the time drifting around the Earth. Their energies are also enhanced, the majority of which reach up to 100 keV. On the other hand, 18.56% of the total test particles are precipitated (Figure 2h) during the simulation time, and on average, they can survive for about 5 min before colliding with the upper atmosphere. Their final energy distribution peaks at approximately 150 keV as they reach at 800 km.

Figure 3 displays particle trajectories at 774.5 ka in the middle stage of the reversal and the energy distributions of both trapped and precipitated particles. Notably, the ion trajectories differ considerably from that in a dipolar configuration. Most particles do not exhibit a discernible drift motion after crossing the boundary at $r = 6$ Re but move directly toward the Earth. In the group of "trapped" particles (Figure 3b), some particles demonstrate brief bouncing and drifting trajectories upon reaching specific regions around the Earth, but no distinct drift shell is observed. These results suggest that during the period of paleomagnetic reversal, the traditionally trapped radiation belt or ring current may not exist. On the other hand, the precipitated particles display trajectories directed toward the Earth, as seen in Figure 3c. It appears that these particles precipitate into the Earth's atmosphere at a faster and more direct way than those at 765 ka (Figure 2c). Figure 3d demonstrates that the magnetospheric configuration at 774.5 ka is not axisymmetric near the Earth. Multiple magnetic poles are irregularly distributed on the Earth's surface. This chaotic distribution of magnetic field lines causes the precipitation to exhibit a globally distributed pattern (Figure 3e), instead of concentrating near high latitudes like in the other case. Such a global distribution of precipitation may produce auroras on a worldwide scale.

The energy distribution of magnetospheric particles at 774.5 ka is illustrated in Figure 3f. While the initial energy distribution of particles still ranges from 10^1–10^5 eV, the bulk distribution of the peak energy along their trajectories only increases by about one order of magnitude, a much smaller increment compared to that at 765 ka. At 774.5 ka, the irregular geomagnetic field, dominated by non-dipolar components, significantly impacts the magnetospheric configuration. Consequently, such interference prevents one from observing as evident acceleration phenomena as in the other case. Furthermore, we found that in comparison to the over 65% of "trapped" particles in the other case, only 2.5% of the total particles are "trapped" (Figure 3g). Additionally, their average "trapped" time was reduced to 918.51 s (trapped until the end of the simulation), and the bulk energy change during their motion inside the $r = 6$ Re boundary is insignificant. This means that the irregular

Figure 2. The characteristics of particle motion at 765 ka. Panel (a) shows the trajectories of selected particles, where the blue line represents the "trapped" particles and the red line represents the "precipitating" particles. Panel (b) shows an example trajectory of a "trapped" particle. The red dotted line represents the equatorial projection of the trajectory. Panel (c) shows an example trajectory of a "precipitating" particle. The red dotted line represents the equatorial projection of the trajectory. Panel (d) shows the magnetic field line configuration of the background magnetosphere, where the color on the surface of the central spherical shell represents the global distribution of the Br component of the geomagnetic field on the Earth's surface. Panel (e) displays the global distribution of precipitated particles by red cycles. The color on the surface shows the intrinsic magnetic field component (Br). Panel (f) shows the energy distribution of all test particles during their motion in the magnetosphere. The blue histogram represents the initial energy distribution and the red one represents the distribution of maximum energies during the motion of particles. Panel (g) shows the energy distributions of "trapped" particles. The blue histogram represents their energy distribution as they cross the $r = 6$ Re boundary and the red one represents their final energy (The final location is at the end of the simulation). Panel (h) shows the energy distributions of "precipitating" particles. The histograms represent the same meaning as (g), the final location is at the upper atmosphere where the particle precipitates.

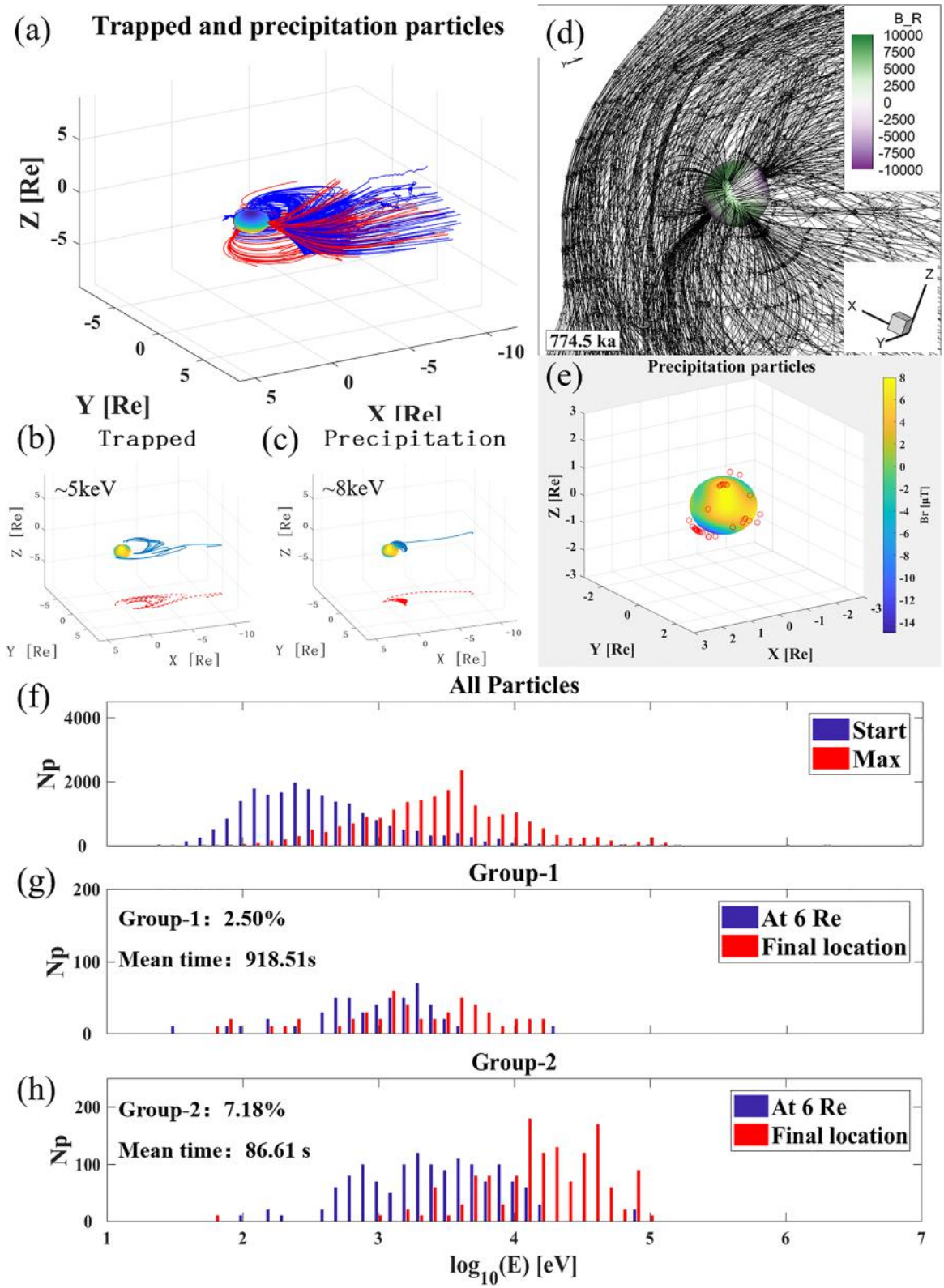

Figure 3. The characteristics of particle motion at 774.5 ka. The figures are in the same format as Figure 2.

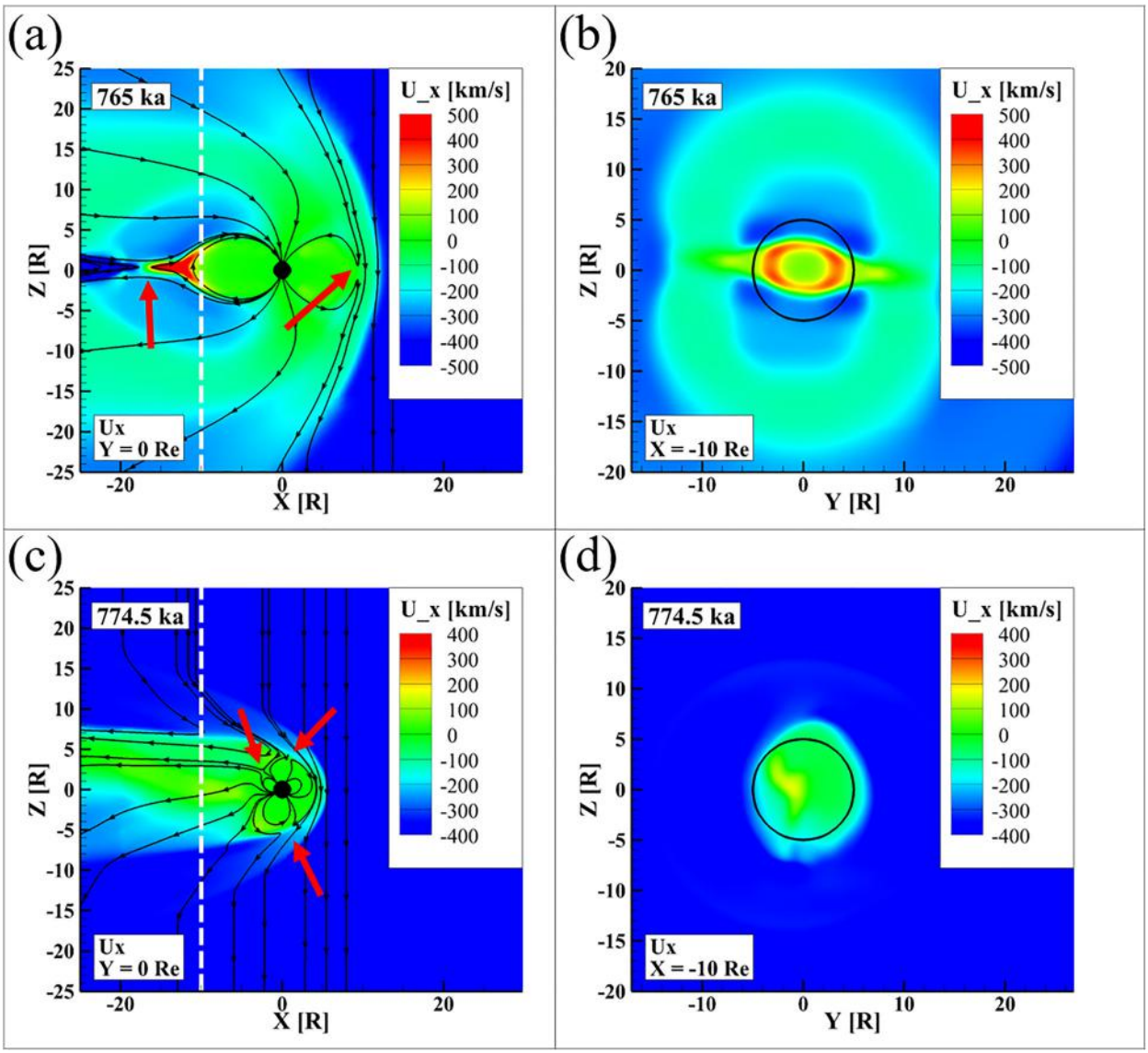

Figure 4. (a, b) show the earthward velocity (U_x) in the noon-midnight meridian plane (a) and in the YZ plane at $X_{GSM} = -10$ Re (b) at 765 ka. (c, d) show the same characteristics at 774.5 ka. The black lines in (a, c) represent magnetic field lines. The black circles in (b, d) represent the zone where the particles are initially released.

field cannot sustain the trapped particles for an extended period, nor can it bring substantial acceleration on the particles. In Figure 3h, the energy distribution of precipitated particles in their final positions (at 800 km above the surface) shifts to higher energies, indicating a net energy gain while traveling from the 6 Re boundary to the upper atmosphere. The proportion of precipitated particles is about 7%, much less than that at 765 ka, and their survival time is also shorter.

From the above results, we can see that particles at different reversal phases experienced different acceleration processes in the magnetotail. Figure 4 shows the Earthward velocity U_x from the two MHD simulations within the noon-midnight meridian plane and YZ plane. At 765 ka, the magnetotail reconnection site (points by red arrows on the left) lies approximately at $X_{GSM} = -20$ Re, resulting in clear Earthward and tailward plasma flows (Figure 4a). The white dashed line marks at $X_{GSM} = -10$ Re, where the particles are initially released within the circler zone as indicated in Figure 4b. The fast Earthward plasma flow stems from the reconnection outflow region and starts to move along magnetic field lines when encountering a more dipolar inner magnetosphere. Figure 4b shows a ring-type distribution of the fast flow at $X_{GSM} = -10$ Re in the YZ plane, indicating a wide access of particles toward the Earth. Such a wide and fast flow explains why more than 65% of the particles

arrive at the inner magnetosphere and why the particle acceleration is profound throughout the simulation. In contrast, the situation during the reversal phase at 774.5 ka was significantly different. Figure 4c displays that the geomagnetic field is in a non-symmetric multipolar state, and the magnetic reconnection site which points by red arrows does not appear in the magnetotail beyond $X_{GSM} = -10$ Re. Instead, multiple reconnection sites are irregularly distributed near the Earth inside $r = 6$ Re. Consequently, the Earthward plasma flow is very weak at $X_{GSM} = -10$ Re where the particles are initially released (see Figure 4d). Therefore, not only does the proportion of earthward-moving particles decrease, but the magnetic field structure in the inner magnetosphere is also hard to trap particles from the magnetotail.

4. Summary

In this study, we simulated the motion of charged particles under different magnetospheric configurations during the Matuyama-Brunhes (M-B) geomagnetic reversal. The SWMF model was employed to simulate the solar wind interaction with the geomagnetic field, either dipolar or dominant by multipoles during the M-B reversal. We conducted particle tracing simulations in the magnetosphere after launching particles at $X_{GSM} = -10$ Re following a Kappa energy distribution. It is found that within the magnetosphere dominant with a dipole-like intrinsic geomagnetic field, particles experience pronounced acceleration while traveling Earthward from the magnetotail, and over 65% of the particles flowing from the magnetotail region enter the inner magnetosphere and are trapped. However, in the middle of the polarity reversal, only 2.5% of the particles are trapped in the inner magnetosphere within the simulation time period, and their trapping time was considerably reduced. These particles gain very little net energy while traveling Earthward. These above differences can be attributed to the changes in the geomagnetic field configuration and the disappearance of stable drift shells in the polarity reversal phase. Our simulations, therefore, suggest that a more dipolar field was conducive to "trapping" and accelerating particles.

We also traced the particle precipitating process under the two configurations. It is found that the proportion of precipitating particles during the reversal phase decreases, and their surviving duration in the magnetosphere is shorter, as opposed to the case with a dipole-dominant geomagnetic field. Moreover, the occurrence of precipitation changes from high-latitude polar regions to a worldwide distribution, appearing even in mid-to-low latitude regions. The energy gain of the precipitating particles is also lower than that with a dipolar configuration. This suggests that the change in the structure of the magnetosphere during the reversal and the lack of bouncing and drift motions lead to faster precipitation of particles in the magnetosphere to lower latitudes and broader areas on the Earth's surface. However, the Earth's magnetic field during the reversal greatly weakens the shielding effect of the Earth's magnetosphere from the solar wind (Gong et al., 2022). This means more heating in the upper atmosphere, which could change the global climate. This study therefore also provides some insights into the comparative study of other planets, such as Mars which does not possess an intrinsic global dipole field.

It should be noted that due to a finite simulation time, we can only illustrate the trajectories of charged particles for a restricted duration. If we increase the simulation time, the trapping time of "trapped" particles and the percentage of the two types of particles are expected to change. The simulation duration could heavily impacts the drift duration of the "trapped" ions. At 765 ka, the Earth's magnetic field resembles a dipolar field and can result in a stable drift shell within the inner magnetosphere, allowing for a long-term trapping of charged particles from the magnetotail. Thus, the 1,177.4 s trapping time in the current study only indicates the stable trapping of particles in the inner magnetosphere within the limited simulation time. Conversely, at 774.5 ka, the irregular magnetosphere can hardly trap particles for an extended period. The percentage of precipitating particles will increase if the simulation extends longer. Therefore, the quantitative values in the current study may alter to some extent. Nonetheless, we believe that the conclusion of this study still remains. That is, in the polarity reversal phase, the trapping of charged particles can hardly survive for long and the precipitation occurs globally.

Data Availability Statement

The modeling tools described in this publication are available online: https://github.com/MSTEM-QUDA. The simulation data are archived at https://doi.org/10.5281/zenodo.7757158.

Acknowledgments
This work is supported by the NSFC Grants 41821003 and 41974192, and by the Fundamental Research Funds for the Central Universities. This work was carried out using the SWMF and BATS-R-US tools developed at the University of Michigan's Center for Space Environment Modeling (CSEM). Simulations were performed over the Tianhe-2 National Supercomputer Center at Guangzhou, China.

References

Amit, H., Leonhardt, R., & Wicht, J. (2010). Polarity reversals from paleomagnetic observations and numerical dynamo simulations. *Space Science Reviews*, *155*(1–4), 293–335. https://doi.org/10.1007/s11214-010-9695-2

Brizard, A. J., & Chan, A. A. (1999). Nonlinear relativistic gyrokinetic Vlasov-Maxwell equations. *Physics of Plasmas*, *6*(12), 4548–4558. https://doi.org/10.1063/1.873742

Cande, S. C., & Kent, D. V. (1995). Revised calibration of the geomagnetic polarity timescale for the Late. *Cretaceous and Cenozoic*, *100*(B4), 6093–6095. https://doi.org/10.1029/94JB03098

Cary, J. R., & Brizard, A. J. (2009). Hamiltonian theory of guiding-center motion. *Reviews of Modern Physics*, *81*(2), 693–738. https://doi.org/10.1103/RevModPhys.81.693

Channell, J. E. T., Xuan, C., & Hodell, D. A. (2009). Stacking paleointensity and oxygen isotope data for the last 1.5 Myr (PISO-1500). *Earth and Planetary Science Letters*, *283*(1–4), 14–23. https://doi.org/10.1016/j.epsl.2009.03.012

Gao, J., Korte, M., Panovska, S., Rong, Z., & Wei, Y. (2022). Effects of the laschamps excursion on geomagnetic cutoff rigidities. *Geochemistry, Geophysics, Geosystems*, *23*(2), e2021GC010261. https://doi.org/10.1029/2021GC010261

Glassmeier, K.-H., & Vogt, J. (2010). Magnetic polarity transitions and biospheric effects. In G. Hulot, A. Balogh, U. R. Christensen, C. Constable, M. Mandea, & N. Olsen (Eds.), *Terrestrial magnetism. Series: Space sciences series of ISSI* (Vol. 36, pp. 387–410). https://doi.org/10.1007/978-1-4419-7955-1_14

Gong, F., Yu, Y., Cao, J., Wei, Y., Gao, J., Li, H., et al. (2022). Simulating the solar wind-magnetosphere interaction during the Matuyama-Brunhes paleomagnetic reversal. *Geophysical Research Letters*, *49*(3), e97340. https://doi.org/10.1029/2021GL097340

Hudson, M. K., Kress, B. T., Mueller, H.-R., Zastrow, J. A., & Bernard Blake, J. (2008). Relationship of the Van Allen radiation belts to solar wind drivers. *Journal of Atmospheric and Solar-Terrestrial Physics*, *70*(5), 708–729. https://doi.org/10.1016/j.jastp.2007.11.003

Jackson, A., & Finlay, C. C. (2007). Geomagnetic secular variation and its applications to the core. In G. Schubert (Ed.), *Geomagnetism* (Vol. 5, pp. 147–193). https://doi.org/10.1016/B978-044452748-6.00090-0

Jacobs, J. A. (2005). Reversals of the Earth's magnetic field.

Kirpichev, I. P., Antonova, E. E., Stepanova, M., Eyelade, A. V., Espinoza, C. M., Ovchinnikov, I. L., et al. (2021). Ion Kappa distribution parameters in the magnetosphere of the Earth at geocentric distances smaller than 20 RE during quiet geomagnetic conditions. *Journal of Geophysical Research: Space Physics*, *126*(10), e29409. https://doi.org/10.1029/2021JA029409

Korte, M., Brown, M. C., Panovska, S., & Wardinski, I. (2019). Robust characteristics of the Laschamp and Mono Lake geomagnetic excursions: Results from global field models. *Frontiers in Earth Science*, *7*, 86. https://doi.org/10.3389/feart.2019.00086

Korte, M., & Mandea, M. (2019). Geomagnetism: From Alexander von humboldt to current challenges. *Geochemistry, Geophysics, Geosystems*, *20*(8), 3801–3820. https://doi.org/10.1029/2019GC008324

Kress, B. T., Hudson, M. K., Looper, M. D., Albert, J., Lyon, J. G., & Goodrich, C. C. (2007). Global MHD test particle simulations of ¿10 MeV radiation belt electrons during storm sudden commencement. *Journal of Geophysical Research: Space Physics*, *112*(A9), A09215. https://doi.org/10.1029/2006JA012218

Laj, C., & Channell, J. (2015). 5.10 - Geomagnetic excursions. In G. Schubert (Ed.), *Treatise on geophysics* (2nd ed. ed., pp. 343–383). Elsevier. https://doi.org/10.1016/B978-0-444-53802-4.00104-4

Leonhardt, R., & Fabian, K. (2007). Paleomagnetic reconstruction of the global geomagnetic field evolution during the Matuyama/Brunhes transition: Iterative Bayesian inversion and independent verification. *Earth and Planetary Science Letters*, *253*(1–2), 172–195. https://doi.org/10.1016/j.epsl.2006.10.025

Lowrie, W., & Kent, D. V. (2004). Geomagnetic polarity timescales and reversal frequency regimes. *Washington DC American Geophysical Union Geophysical Monograph Series*, *145*, 117–129. https://doi.org/10.1029/145GM09

Merrill, R. T., McElhinny, M. W., McFadden, P. L., & Banerjee, S. K. (1997). The magnetic field of the Earth: Paleomagnetism, the core, and the deep mantle. *Physics Today*, *50*(9), 70. https://doi.org/10.1063/1.881919

Powell, K. G., Roe, P. L., Linde, T. J., Gombosi, T. I., & De Zeeuw, D. L. (1999). A solution-adaptive upwind scheme for ideal magnetohydrodynamics. *Journal of Computational Physics*, *154*(2), 284–309. https://doi.org/10.1006/jcph.1999.6299

Ridley, A., Gombosi, T., & Dezeeuw, D. (2004). Ionospheric control of the magnetosphere: Conductance. *Annales Geophysicae*, *22*(2), 567–584. https://doi.org/10.5194/angeo-22-567-2004

Ridley, A. J., De Zeeuw, D. L., & Rastätter, L. (2016). Rating global magnetosphere model simulations through statistical data-model comparisons. *Space Weather*, *14*(10), 819–834. https://doi.org/10.1002/2016SW001465

Shea, M. A., & Smart, D. F. (2004). Preliminary study of cosmic rays, geomagnetic field changes and possible climate changes. *Advances in Space Research*, *34*(2), 420–425. https://doi.org/10.1016/j.asr.2004.02.008

Singer, B. S. (2014). A quaternary geomagnetic instability time scale. *Quaternary Geochronology*, *21*, 29–52. (Quaternary Geochronology Special Issue: Advances in 40Ar/39Ar Dating of Quaternary Events and Processes). https://doi.org/10.1016/j.quageo.2013.10.003

Singer, B. S., Hoffman, K. A., Coe, R. S., Brown, L. L., Jicha, B. R., Pringle, M. S., & Chauvin, A. (2005). Structural and temporal requirements for geomagnetic field reversal deduced from lava flows. *Nature*, *434*(7033), 633–636. https://doi.org/10.1038/nature03431

Singer, B. S., Jicha, B. R., Mochizuki, N., & Coe, R. S. (2019). Synchronizing volcanic, sedimentary, and ice core records of Earth's last magnetic polarity reversal. *Science Advances*, *5*(8), eaaw4621. https://doi.org/10.1126/sciadv.aaw4621

Smart, D. F., & Shea, M. A. (2009). Fifty years of progress in geomagnetic cutoff rigidity determinations. *Advances in Space Research*, *44*(10), 1107–1123. https://doi.org/10.1016/j.asr.2009.07.005

Stadelmann, A., Vogt, J., Glassmeier, K.-H., Kallenrode, M.-B., & Voigt, G.-H. (2010). Cosmic ray and solar energetic particle flux in paleomagnetospheres. *Earth Planets and Space*, *62*(3), 333–345. https://doi.org/10.5047/eps.2009.10.002

Tóth, G., Sokolov, I. V., Gombosi, T. I., Chesney, D. R., Clauer, C. R., de Zeeuw, D. L., et al. (2005). Space weather modeling framework: A new tool for the space science community. *Journal of Geophysical Research: Space Physics*, *110*(A12), A12226. https://doi.org/10.1029/2005JA011126

Tóth, G., van der Holst, B., Sokolov, I. V., De Zeeuw, D. L., Gombosi, T. I., Fang, F., et al. (2012). Adaptive numerical algorithms in space weather modeling. *Journal of Computational Physics*, *231*(3), 870–903. https://doi.org/10.1016/j.jcp.2011.02.006

Valet, J.-P., & Fournier, A. (2016). Deciphering records of geomagnetic reversals. *Reviews of Geophysics*, *54*(2), 410–446. https://doi.org/10.1002/2015RG000506

Valet, J.-P., Fournier, A., Courtillot, V., & Herrero-Bervera, E. (2012). Dynamical similarity of geomagnetic field reversals. *Dynamical Similarity of Geomagnetic Field Reversals*, *490*(7418), 89–93. https://doi.org/10.1038/nature11491

Valet, J.-P., Meynadier, L., & Guyodo, Y. (2005). Geomagnetic dipole strength and reversal rate over the past two million years. *Nature*, *435*(7043), 802–805. https://doi.org/10.1038/nature03674

Welling, D. T., & Ridley, A. J. (2010). Exploring sources of magnetospheric plasma using multispecies MHD. *Journal of Geophysical Research: Space Physics*, *115*(A4), A04201. https://doi.org/10.1029/2009JA014596

Yu, Y., Jordanova, V., Zou, S., Heelis, R., Ruohoniemi, M., & Wygant, J. (2015). Modeling subauroral polarization streams during the 17 March 2013 storm. *Journal of Geophysical Research: Space Physics*, *120*(3), 1738–1750. https://doi.org/10.1002/2014JA020371

Yu, Y., & Ridley, A. J. (2008). Validation of the space weather modeling framework using ground-based magnetometers. *Space Weather*, *6*(5), 05002. https://doi.org/10.1029/2007SW000345

Yu, Y., Ridley, A. J., Welling, D. T., & Tóth, G. (2010). Including gap region field-aligned currents and magnetospheric currents in the MHD calculation of ground-based magnetic field perturbations. *Journal of Geophysical Research: Space Physics*, *115*(A8), A08207. https://doi.org/10.1029/2009JA014869